INSTITUTE OF PHYSICS PUBLISHING NETWORK: COMPUTATION IN NEURAL SYSTEMS

Network: Comput. Neural Syst. **13** (2002) 381–395 PII: S0954-898X(02)38849-3

Analysis of tubular structures in three-dimensional confocal images

Geert J Streekstra[1,3] **and Jaap van Pelt**[2]

[1] Department of Medical Physics, Academic Medical Center, Meibergdreef 9, 1105 AZ Amsterdam, The Netherlands
[2] Netherlands Institute for Brain Research, Meibergdreef 33, 1105 AZ Amsterdam, The Netherlands

E-mail: g.j.streekstra@amc.uva.nl

Received 14 January 2002
Published 30 July 2002
Online at stacks.iop.org/Network/13/381

Abstract

Knowledge about the relationship between morphology and the function of neurons is an important instrument in understanding the role that neurons play in information processing in the brain. In paricular, the diameter and length of segments in dendritic arborization are considered to be crucial morphological features. Consequently, accurate detection of morphological features such as centre line position and diameter is a prerequisite to establish this relationship.

Accurate detection of neuron morphology from confocal microscope images is hampered by the low signal to noise ratio of the images and the properties of the microscope point spread function (PSF). The size and the anisotropy of the PSF causes feature detection to be biased and orientation dependent.

We deal with these problems by utilizing Gaussian image derivatives for feature detection. Gaussian kernels provide for image derivative estimates with low noise sensitivity. Features of interest such as centre line positions and diameter in a tubular neuronal segment of a dendritic tree can be detected by calculating and subsequently utilizing Gaussian image derivatives. For diameter measurement the microscope PSF is incorporated into the derivative calculation.

Results on real and simulated confocal images reveal that centre line position and diameter can be estimated accurately and are bias free even under realistic imaging conditions.

1. Introduction

In neuroscience, knowledge regarding the relationship between neural morphology and function is considered to be of key importance to gain insight into the working principles of neural structures [1–3]. Morphological features of biological interest manifest themselves

[3] Author to whom any correspondence should be addressed.

at different spatial scales [1]. At intermediate scales features of interest are the spatial coverage, shape complexity measures (e.g. integrated curvature) and the dendrogram representation of a neuron. These features are used for classification into different cell classes that can be related to differences in physiological behaviour [3]. At a smaller scale the shape and size of individual neuronal segments combined with the dendrogram are crucial to relate electrical signal processing in the dendritic tree to neuron morphology. In the modelling of the electrical behaviour of the neuron the 3D positions of segments and bifurcations with respect to each other are usually not incorporated. Full 3D reconstruction of the neuron would allow more realistic electrical modelling for cases where electrical interaction between different parts of the structure is substantial.

Basic features consisting of the topology of the neuron (i.e. the dendrogram), the positions of the centreline of the segments constituting the skeleton of the tree, the diameter at each centre line position and the positions of bifurcations and end points of segments are sufficient to derive the morphological and electrical features mentioned above.

A number of methods are available to detect centre lines in tubular structures from 3D images. Two representative examples in medicine and biology are medial axis determination methods in a colon [4] and in chromosomes [5] respectively. These methods are based on widely used topology preserving thinning methods in binary images. These methods heavily rely on thresholding. The extraction, however, of basic features from 3D confocal microscope images turns out to be complicated by noise and distortions present in real images. Moreover, the intensity levels of the neural segments as present in the image may vary along the neural tree. Consequently, thresholding the image is often unreliable and makes utilization of grey value information a prerequisite for accurate feature detection.

Although feature extraction methods as implemented in commercial products are available, they are usually also based on a thresholded image. Therefore the performance of these methods is not optimal and improvements on these methods are required.

The resolution of the optics in a confocal microscope is characterized by its 3D point spread function (PSF). The dimensions of the PSF resemble the lower limit of object sizes that can be properly imaged. The PSF causes the appearance of a small object in the image to be blurred compared to the real object in the sample. In confocal images of neuron cells the diameters of the neural segments may be of the same order of magnitude as the size of the microscope PSF. Consequently, neural segments will appear blurred in the image. The blurring will influence diameter measurement and introduce a bias in the diameter estimates. An appropriate method for diameter measurement from confocal images should therefore take the influence of the PSF on the diameter estimate into account. However, current methods for diameter measurement omit the influence of the PSF and therefore yield biased results.

In this paper we focus our attention on the detection of basic features of 3D tubular structures as they appear in 3D confocal images [6]. The feature extraction methods we describe are based on a combination of scale space theory and differential geometrical principles [7–11]. We show that these grey value based methods provide for an accurate and automatic detection of centre line position and diameter of tubular structures. A second topic we investigate is the magnitude of the bias introduced by the microscope PSF in the diameter measurement and we present a method to correct for it.

2. Detection of morphological features in tubular structures

2.1. Image derivatives for feature detection

The methods that we present for feature extraction are based on the use of spatial derivatives of the intensity function $I(x, y, z)$ representing the image. In practice these spatial derivatives are calculated from the 3D image data as obtained with the confocal microscope.

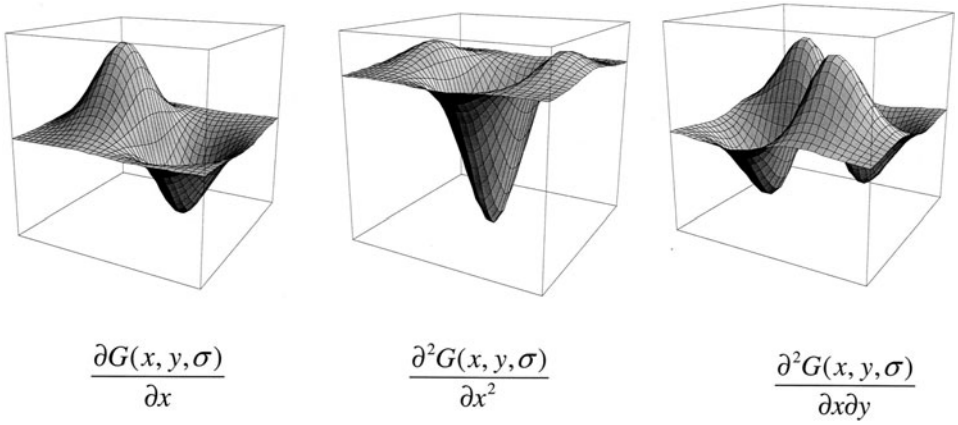

Figure 1. First- and the second-order Gaussian derivatives kernels for 2D images. A kernel represents the relative weighting of the pixels within the area that is used for the calculation of the image derivatives.

An approximation of a first-order spatial derivative in an image $I(x, y, z)$ can be obtained by computing the intensity difference of two adjacent voxels. The disadvantage of this method is that the resulting derivative estimates are sensitive to the noise in the intensity values of the individual voxels. A better way is to use more voxels in the neighbourhood of the point (x, y, z) where the derivative has to be calculated. This can be realized by convolving the image with a derivative kernel. In our methods we use the derivative of a Gaussian as the derivative kernel. Figure 1 shows the shape of the first- and the second-order Gaussian derivative kernels for calculation of image derivatives in 2D images $I(x, y)$. A kernel represents the relative weighting of the pixels within the area that is used for the calculation of the image derivatives. By convolving the image with a Gaussian derivative kernel the image derivative is effectively calculated in an image $I(x, y, \sigma)$ which is the original image $I(x, y)$ smoothed by a Gaussian $G(x, y, \sigma)$. This is due to the associativity of the linear derivative and convolution operators, e.g.

$$\frac{\partial}{\partial x}(I(x, y) * G(x, y, \sigma)) = I(x, y) * \frac{\partial G(x, y, \sigma)}{\partial x}, \tag{1}$$

where $*$ denotes the convolution operator. The scale parameter σ defines the effective region around a certain point that is used for the calculation of the derivative value.

For 3D images analogue kernels exist. These kernels are not shown here since they cannot be plotted in a single graph as for the 2D case. The 3D derivatives are obtained by convolution of the original image $I(x, y, z)$ with the appropriate Gaussian derivative kernels

$$\begin{aligned} I(x, y, z, \sigma) &= G(x, y, z, \sigma) * I(x, y, z), \\ I_i(x, y, z, \sigma) &= \frac{\partial G(x, y, z, \sigma)}{\partial i} * I(x, y, z), \qquad (i = x, y, z) \\ I_{ij}(x, y, z, \sigma) &= \frac{\partial^2 G(x, y, z, \sigma)}{\partial i \partial j} * I(x, y, z), \qquad (ij = xx, xy, xz, yy, yz, zz) \end{aligned} \tag{2}$$

with

$$G(x, y, z, \sigma) = \frac{1}{(\sqrt{2\pi\sigma^2})^3} \exp\left(-\frac{x^2 + y^2 + z^2}{2\sigma^2}\right). \tag{3}$$

Utilization of Gaussian derivative kernels enables optimal use of grey value information present in the image. The extension of the kernel over a volume around the voxel under consideration provides for derivative values that are rather insensitive to noise and irregularities in the image. By using Gaussian derivatives methods can be developed that are invariant with respect to intensity fluctuations along the dendritic tree. Such methods are based on the shape of the gray value pattern rather than on the absolute intensity values. In the following sections we will demonstrate the usefulness of Gaussian derivative kernels in centre line detection and diameter measurement procedures.

2.2. Centre line detection

The centre line detection method that we propose to use for neuron tracing is based on a method that has been described in previous reports [8–11]. Here we recall the essentials of this derivative based method. Here we recall the essentials of this derivative based method.

The starting point of the method is the analysis of the second-order Gaussian derivatives in the image. At the centre line of tubular structures in an image like that of a neuron the second-order derivative in the centre line direction is much smaller than in the directions perpendicular to the centre line [12, 13]. Another property of a tubular structure in an image is that the first-order derivatives at the centreline vanish. These two properties can be used to find the centre line position.

The second-order derivative property is used to find the direction of the centre line. To this end we estimate all second-order Gaussian derivatives at a certain discrete position $\boldsymbol{P_d}$ in the image. The second-order Gaussian derivatives are used to build the 3×3 Hessian matrix

$$\mathbf{H} = \begin{pmatrix} I_{xx} & I_{xy} & I_{xz} \\ I_{yx} & I_{yy} & I_{yz} \\ I_{zx} & I_{zy} & I_{zz} \end{pmatrix}. \tag{4}$$

Arguments are left out here for brevity. The Hessian matrix $\mathbf{H}$ represents the second-order structure of local intensity variations around the 3D point under observation. From $\mathbf{H}$ we calculate the eigenvalues $\lambda_t, \lambda_n, \lambda_m$ and the corresponding eigenvectors $\boldsymbol{t}$, $\boldsymbol{n}$ and $\boldsymbol{m}$ which form the orthonormal base for a local Cartesian coordinate system. The vector $\boldsymbol{t}$ which is aligned to the line direction (see figure 2) is the eigenvector with the smallest absolute eigenvalue λ_t, i.e.

$$|\lambda_t| \ll |\lambda_n|, |\lambda_m|. \tag{5}$$

In the plane perpendicular to the line direction the grey value distribution can be approximated by a second-order Taylor polynomial

$$I(\xi, \eta) = I + \boldsymbol{p} \cdot \nabla I + \tfrac{1}{2}\boldsymbol{p}^T \cdot \mathbf{H} \cdot \boldsymbol{p}. \tag{6}$$

In equation (6) $\boldsymbol{p}$ is a vector in the plane defined by $\boldsymbol{n}$ and $\boldsymbol{m}$, i.e.

$$\boldsymbol{p} = \xi \boldsymbol{n} + \eta \boldsymbol{m}. \tag{7}$$

I and ∇I are the grey value and gradient vector at the discrete position $\boldsymbol{P_d}$. The position of the centre line $\boldsymbol{P_c}$ relative to $\boldsymbol{P_d}$ is found by setting the gradient of the local Taylor polynomial to zero [9]:

$$\nabla I(\xi, \eta) = \mathbf{0} \tag{8}$$

and solving η and ξ from the resulting linear equation. The actual sub voxel centre line position $\boldsymbol{P_s}$ is calculated by

$$\boldsymbol{P_s} = \boldsymbol{P_d} + \boldsymbol{P_c}. \tag{9}$$

In a discrete image $\boldsymbol{P_s}$ will only be a centre line point if it is within the boundaries of the discrete voxel position $\boldsymbol{P_d}$.

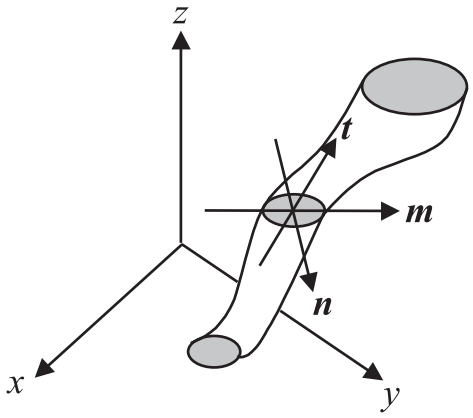

Figure 2. 3D line structure with local eigenvectors $\boldsymbol{t}$, $\boldsymbol{n}$ and $\boldsymbol{m}$ of the Hessian matrix and corresponding eigenvalues $\lambda_t, \lambda_n, \lambda_m$. The eigenvector $\boldsymbol{t}$ with the smallest eigenvalue in magnitude $|\lambda_t|$ is in the local direction of the line.

The centre line detection method mentioned in this section imposes only minor constraints on the shape of the intensity profile across the tube. In images of neurons cross sections are usually close to circular. In a circular cross section $\lambda_m = \lambda_n$ and obviously a single centre line position will be found in this case. For a non-circular cross section the analysis of the Hessian matrix will yield $\lambda_m \neq \lambda_n$. Although λ_m and λ_n may be unequal they are generally non-zero and by utilizing equation (6) a single centre line position will be found. Consequently, the only requirements to be fulfilled for successful centre line detection are equation (5) and a first derivative that vanishes at the centre line. These requirement are usually fulfilled for a tubular structure with arbitrarily shaped cross section.

2.3. Diameter measurement

For diameter estimation it is necessary to take the shape of the 2D grey value profile across the line into account. We assume that the intensity profile $I(r)$ is bounded by the general condition

$$I(r) = \begin{cases} I_0 f(r) & (r \leqslant R) \\ 0 & (r > R). \end{cases} \tag{10}$$

In equation (10) I_0 is the grey value at the centre line and r represents the radial position relative to the centre line. We demand that the first derivative of $f(r)$ vanishes at the centre line.

We use the theoretical scale dependencies of $I(r)$ convolved with a Gaussian and the second Gaussian derivatives of $I(r)$ at the centre line position ($r = 0$) to estimate the line diameter. For this purpose expressions are derived for the Gaussian blurred intensity $I(R, \sigma)$ and the Laplacian $\Delta^{\perp} I(R, \sigma)$ restricted to the span of $\boldsymbol{n}$ and $\boldsymbol{m}$. At the centre line position the convolutions involved in the calculation of $I(R, \sigma)$ and $\Delta^{\perp} I(R, \sigma)$ reduce to simple two-dimensional integrals:

$$I(R, \sigma) = I_0 \int_0^{2\pi} \int_0^R f(r) g(r, \sigma) r \, \mathrm{d}r \, \mathrm{d}\theta \tag{11}$$

$$\Delta^{\perp} I(R, \sigma) = I_0 \int_0^{2\pi} \int_0^R f(r) g_{rr}(r, \sigma) r \, \mathrm{d}r \, \mathrm{d}\theta. \tag{12}$$

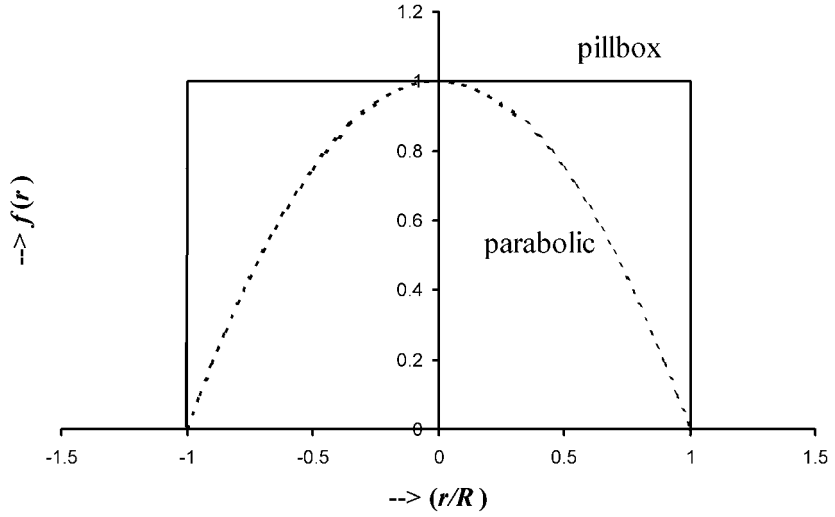

Figure 3. A pillbox shaped and a parabolic line profile.

In (11) and (12) $g(r,\sigma)$ and $g_{rr}(r,\sigma)$ are the 2D Gaussian and its second derivative in the r-direction. The expressions for $I(R,\sigma)$ and the Laplacian $\Delta^{\perp}I(R,\sigma)$ are used to construct a nonlinear filter which is rotation invariant with respect to the line direction and independent of I_0:

$$h(R,\sigma) = -\frac{I(R,\sigma)}{\sigma^2 \frac{1}{2}\Delta^{\perp} I(R,\sigma)}. \tag{13}$$

The denominator in (13) represents the 2D Laplacian based on normalized second derivatives [14].

The theoretical filter output $h(R,\sigma)$ is dependent on the choice of $f(r)$. For a parabolic and a pillbox profile (see figure 3) the integrals appearing in (11) and (12) can be evaluated analytically. For a pillbox profile we find

$$h(q) = \frac{(1-\mathrm{e}^{-q})}{(q\mathrm{e}^{-q})} \tag{14}$$

and for a parabolic profile

$$h(q) = \frac{(1-\mathrm{e}^{-q}) - q}{(q\mathrm{e}^{-q}) - (1-\mathrm{e}^{-q})} \tag{15}$$

with

$$q = \frac{1}{2}\left(\frac{R}{\sigma}\right)^2. \tag{16}$$

Equations (14)–(16) show that for the pillbox and the parabolic profile $h(R,\sigma)$ is only dependent on the dimensionless parameter q that contains both the scale σ of the derivative kernel and the unknown radius R of the line profile.

Figure 4 shows that $h(q)$ is a monotonous increasing function of q. This property makes it possible to estimate q by comparing the filter output h_m measured at scale σ with the theoretical filter function $h(q)$. If h_m is measured and the shape of the profile is known q can be estimated by solving the equation

$$h(q) - h_m = 0. \tag{17}$$

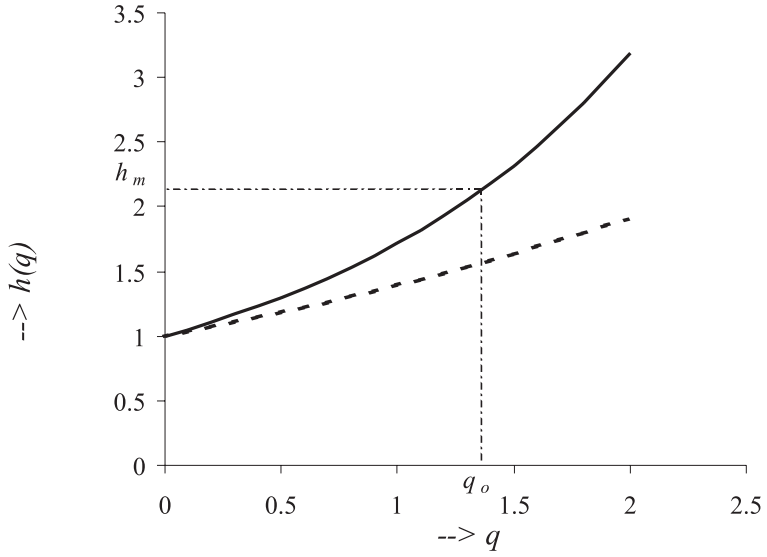

Figure 4. Theoretical line diameter filter output $h(q)$ for a pillbox profile (solid curve) and a parabolic profile (dashed curve). Parameter q is dimensionless and only dependent on R and σ ($q = \frac{1}{2}(R/\sigma)^2$).

By a simple bi-sectioning method the root q_0 of (17) is found. For a given choice of σ the corresponding R is found by solving (16), i.e.

$$R = \sigma\sqrt{2q_0}. \tag{18}$$

2.4. Incorporating the point spread function in the diameter measurement procedure

An accurate diameter measurement in a neuronal segment is of key importance for modelling of the morphological properties of a dendritic tree. Therefore it is necessary to be aware of possible errors in diameter estimation due to the characteristics of the imaging system. A fundamental property of any imaging system is its finite resolution. Resolution significantly influences diameter estimation if it is of the order of magnitude of the diameter of the neuronal segment. This is often the case in practical imaging situations. In a confocal microscope resolution is governed by the 3D point spread function PSF of the system [6]. Ideally the PSF would have zero width. In that case the system correctly images the true fluorochrome distribution in the image. In case of tubular structures the image would represent the neuronal segments as they are present in the sample.

The non-zero width of the PSF, however, causes the tubular structures to appear blurred in the image (figure 5). This is a consequence of the fact that the detected image is a 3D convolution of the tubular objects in the sample (i.e. the fluorochrome distribution) with the microscope PSF. The corresponding intensity profile across the tube in the image is therefore not pillbox shaped any more (see figure 6). The diameter estimation method as presented in the former section will yield a biased estimate since it assumes a pillbox shaped line profile across the tube. Moreover, the anisotropy of the PSF makes the estimated diameter dependent on the orientation of the tubular structure with respect to the imaging axis (see figure 7).

To compensate for the influence of the PSF we incorporate its properties into the diameter measurement method. For that purpose we model the PSF by an anisotropic Gaussian kernel with scale factors $\sigma_{p,l}$ and $\sigma_{p,a}$ in the lateral and axial directions respectively. This is a

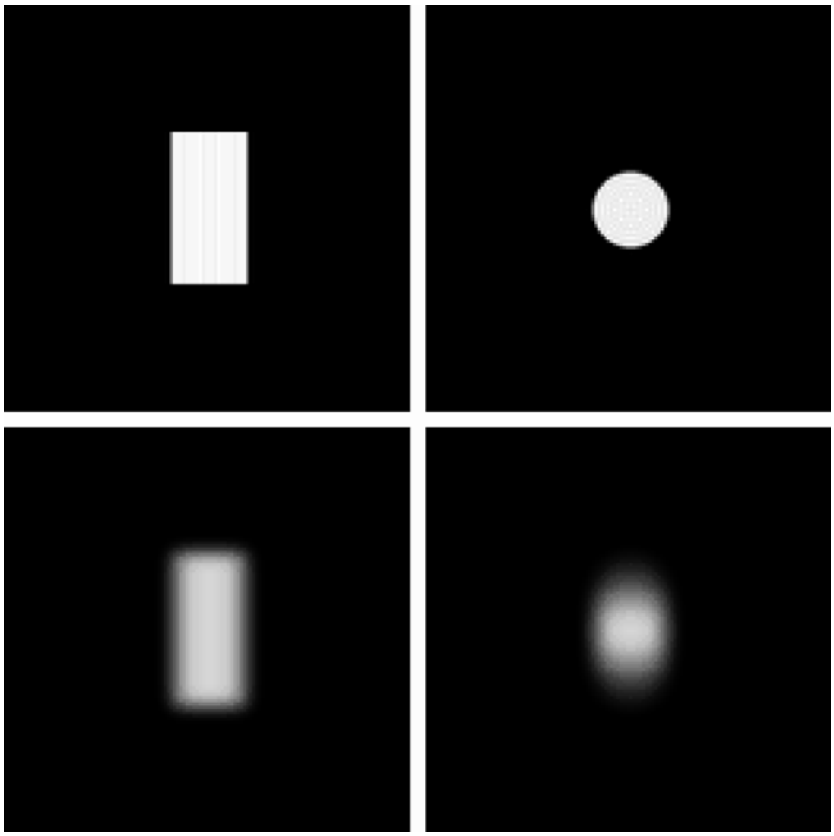

Figure 5. Two orthogonal cross sections of a tubular segment (upper panels: true fluorochrome distribution, lower panels: detected image).

reasonable approximation since a Gaussian closely resembles the shape of a microscope PSF [17]. The Gaussian model is subsequently incorporated into the measurement kernel used for the diameter measurement (cf equations (11) and (12)). The effective measurement kernel is the combination of the Gaussian model of the PSF and an anisotropic Gaussian kernel used in the image derivative calculations. The mathematical relationship between the Gaussian model of the PSF, the kernel used for derivative calculations and the effective isotropic Gaussian measurement kernel $G_e(x, y, z, \sigma_e)$ is

$$G_e(x, y, z, \sigma_e) = G_p(x, y, z, \sigma_{p,l}, \sigma_{p,a}) * G_m(x, y, z, \sigma_{m,l}, \sigma_{m,a}) \tag{19}$$

with

$$\begin{aligned} G_p(x, y, z, \sigma_{p,l}, \sigma_{p,a}) &= \frac{1}{2\pi\sigma_{p,l}^2\sqrt{2\pi}\sigma_{p,a}} \exp\left\{-\frac{1}{2}\left(\frac{x^2+y^2}{\sigma_{p,l}^2} + \frac{z^2}{\sigma_{p,a}^2}\right)\right\}, \\ G_m(x, y, z, \sigma_{m,l}, \sigma_{m,a}) &= \frac{1}{2\pi\sigma_{m,l}^2\sqrt{2\pi}\sigma_{m,a}} \exp\left\{-\frac{1}{2}\left(\frac{x^2+y^2}{\sigma_{m,l}^2} + \frac{z^2}{\sigma_{m,a}^2}\right)\right\}. \end{aligned} \tag{20}$$

In equations (19) and (20) $G_p(x, y, z, \sigma_{p,l}, \sigma_{p,a})$ is the Gaussian model of the microscope PSF and $G_m(x, y, z, \sigma_{m,l}, \sigma_{m,a})$ the measurement kernel that serves as basis for the derivative calculations. The scales $\sigma_{m,l}$ and $\sigma_{m,a}$ are assigned a value that results in an isotropic effective kernel with scale σ_e [18] (see figure 8). The relationship between the scale parameter σ_e of

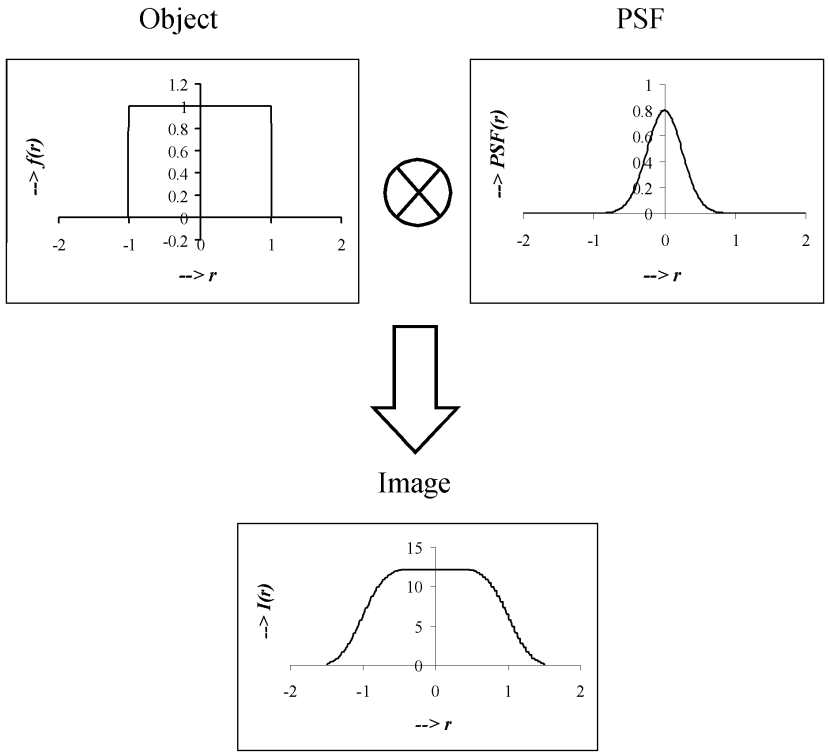

Figure 6. Profiles of radial cross sections of a tubular object, the microscope point spread function ($PSF(r)$) and the resulting image. The profile apparent in the image $I(r)$ is the convolution of the object profile $f(r)$ with $PSF(r)$.

the effective kernel and that of the PSF and the anisotropic measurement kernel ($\sigma_{p,l}$, $\sigma_{p,a}$ and $\sigma_{m,l}$, $\sigma_{m,a}$) is as follows:

$$\sigma_e = \sqrt{\sigma_{p,l}^2 + \sigma_{m,l}^2} = \sqrt{\sigma_{p,a}^2 + \sigma_{m,a}^2}. \tag{21}$$

By choosing σ_e and known values of $\sigma_{p,l}$ and $\sigma_{p,a}$ the values of $\sigma_{m,l}$ and $\sigma_{m,a}$ that have to be applied for the measurement kernels are

$$\begin{aligned} \sigma_{m,l} &= \sqrt{\sigma_e^2 - \sigma_{p,l}^2} \\ \sigma_{m,a} &= \sqrt{\sigma_e^2 - \sigma_{p,a}^2}. \end{aligned} \tag{22}$$

The scale σ_e of the effective kernel is used in (11)–(18) for the diameter estimation.

3. Results

3.1. Centre line detection

The applicability of the centre line detection method is illustrated in two different examples of 3D biological tubular structures (figure 9). The images were obtained using a confocal microscope. The centre line positions were detected by tracing along the axis of the tubular structure. After manual setting an initial position in the tubular structure subsequent centre line

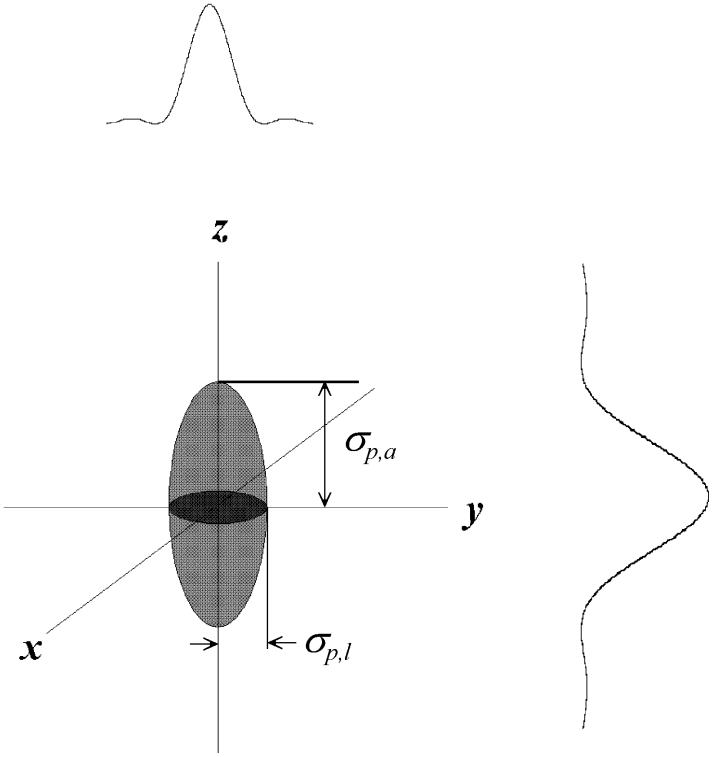

Figure 7. The shape of PSF of a confocal microscope with a high numerical aperture lens. The PSF is approximated by a 3D Gaussian with scales $\sigma_{p,l}$ and $\sigma_{p,a}$ in the lateral and axial directions respectively.

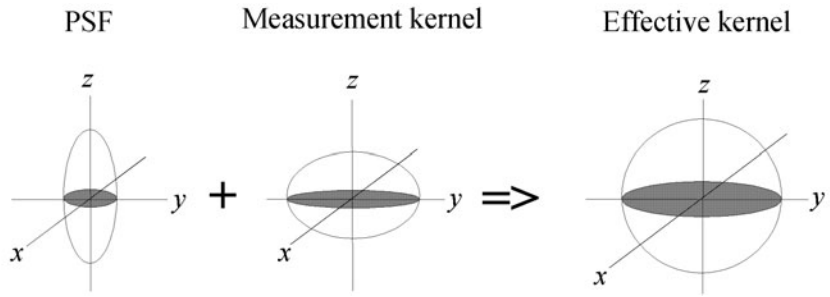

Figure 8. Shapes of the PSF, the anisotropic measurement kernel that serves as a basis for the derivative calculations and the effective isotropic kernel used for diameter estimation.

positions were found by taking a step into the line direction and application of the centre line detection method. The experiments reveal that the centre line estimation method converges to the optimal centre line position as long as the scale of the differentiation kernels was chosen larger than the radius R of the intensity profile across the line. Taking this constraint imposed on the scale into account the method is capable of measuring centre line positions even in the noisy image of the neuron cell (figure 9, right image). In the image of the Spathiphyllum pollen grain (figure 9, left image) the method allows for tracing highly curved line segments.

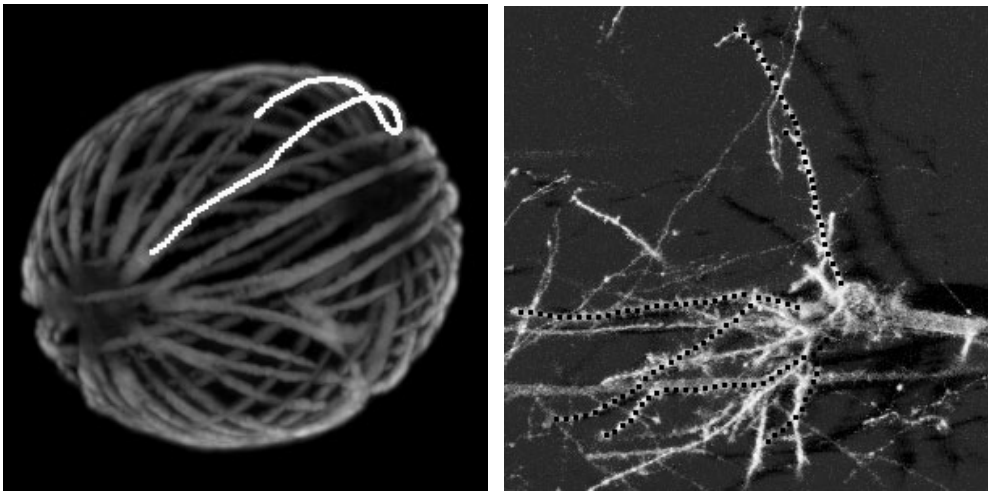

Figure 9. Tracing results in 3D images of a biological specimen (left: a Spathiphyllum pollen grain, right: a pyramidal neuron cell). The images were obtained using a confocal microscope. The black dots in the right panel represent the estimated centre line positions.

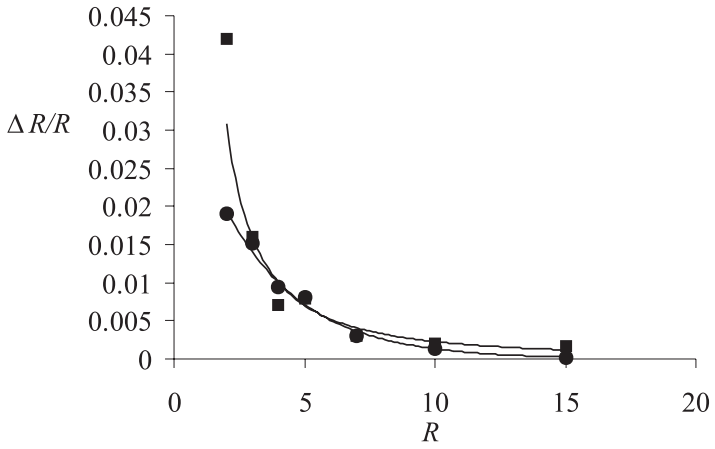

Figure 10. Relative bias in estimation of radius R of the line structure as a function of R. The squares and the dots represent measurements on tubular structures with a pillbox and a parabolic profile respectively.

3.2. Diameter measurement

To evaluate the performance of the line diameter estimation method synthetic images containing straight line segments with circular cross section were used (see figure 5, upper panels). The diameter of the line segment was varied between 2 and 15 voxels. Both pillbox shaped and parabolic intensity profiles were evaluated. The diameter estimate turned out to be independent of the setting of σ in the range where $0.2 < R/\sigma > 2$. In the synthetic images the bias in the estimated diameter is always below 5% (see figure 10).

The diameter measurement procedure was also tested on a biological 3D image from a confocal microscope containing a Spathiphyllum pollen grain (figure 9, left panel). The

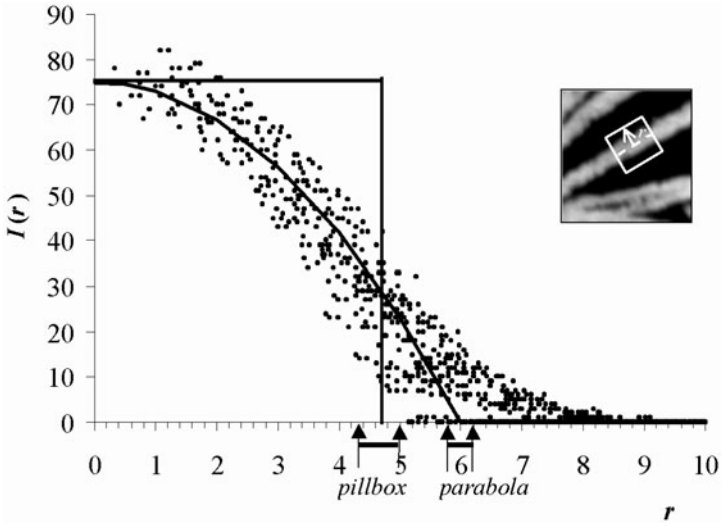

Figure 11. Results of diameter measurement of a tubular structure in a confocal image. The dots are intensity values $I(r)$ as a function of the distance from r from the centre line position. The intensity values $I(r)$ are obtained from a cylindrical volume element with its axis coinciding with the centre line. The scale used for the derivative estimations was varied between 2.0 and 5.0. The vertical arrows along the x-axis indicate the outer limits of the range of the diameter measurements using a pillbox profile (left) and a parabolic profile (right).

diameter was measured at scales varying between 2.0 and 5.0. Within this range of scales the diameter measurement deviates only 6% for the parabolic profile as a model used (figure 11).

In case the pillbox profile is used the diameter measurement procedure fails since the profile is obviously not pillbox shaped. As can be seen in figure 11, the parabola also does not correctly resemble the shape of the measured intensity profile across the tubular structure. Assuming that the fluorochrome is homogeneously distributed in the tubular structure the effect of the microscope PSF is clearly visible in the image data (cf figure 6). Similar effects were observed in tubular segments of neuron cells.

The large spread in the intensity data is partly due to noise and partly to the anisotropy of the PSF. This practical example of a biological sample shows that for accurate measurement the PSF should be taken into account.

To investigate the possible influence of the PSF on the diameter measurement we estimated diameters in synthetic images of tubular structures as shown in figure 5. In all experiments the true diameter R_0 was chosen to be 5.0 and the ratio between the axial size of the PSF ($\sigma_{p,a}$) and the lateral size ($\sigma_{p,l}$) was chosen to be 3.0 as for a high-aperture microscope objective. In our experiments we varied the size of the PSF relative to the radius R of the tube. We also varied the scale σ of the isotropic derivative kernels.

As can be expected the bias in the diameter estimate increases with the size of the PSF (figure 12). In addition, the size of the derivative kernel relative to R is of importance. The bias increases with the σ/R ratio.

Figure 13 shows that the effect of the PSF on the diameter measurement can be excluded by choosing the appropriate anisotropic derivative kernels. In the experiments synthetic tubular objects were used with values for $\sigma_{p,l}/R_0$ of 0.0 and 0.2. 25% Gaussian noise was added to the images to create image data that represents realistic imaging conditions. If the scales $\sigma_{m,l}$ and $\sigma_{m,a}$ are chosen correctly such that the effective kernel is isotropic the estimated value of

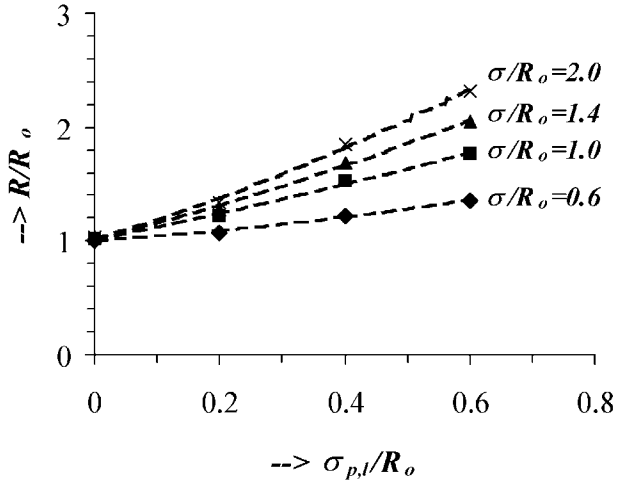

Figure 12. Bias in the diameter measurement as a function of the size of the microscope PSF. The ratio of the scale σ of the isotropic measurement kernel and R_0 is varied between 0.6 and 2.0. Each diameter value represented in the graph is an average of 128 individual measurements.

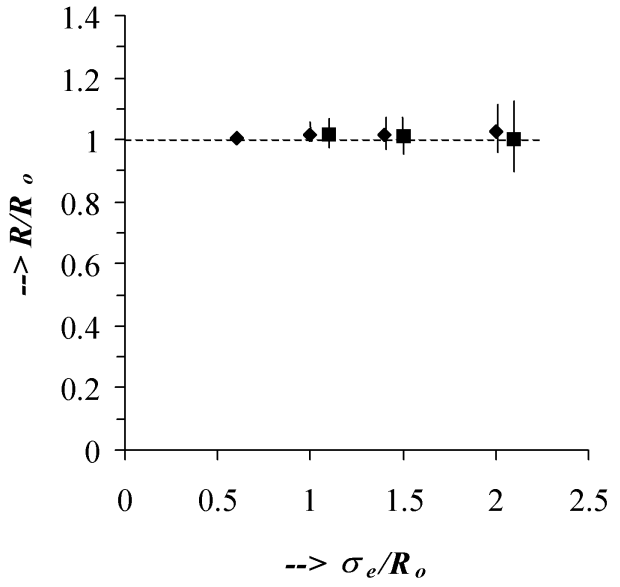

Figure 13. Bias free diameter measurement with properly chosen anisotropic derivative kernels. 25% Gaussian noise was added to the original tubular object (diamonds) and the tubular object blurred with $\sigma_{p,l}/R_0 = 0.2$ (squares).

R is close to the true value R_0. The results that represent average data from 128 centre line positions for each diameter measurement show that the Gaussian derivative kernel effectively suppress the noise present in the images.

4. Discussion

Accurate detection of basic features such as the centre line position and diameter in neuronal structures from confocal images are a prerequisite for reliable reconstruction of neuronal trees and proper modelling of their electrophysiological behaviour. Existing reconstruction systems are limited with respect to accurate and reliable measurement of these features.

In this paper we focused on improved detection methods for detection of the centre line position and diameter in neuronal segments as observed in 3D images acquired with a confocal microscope.

We demonstrated that Gaussian image derivatives can be employed for feature detection in 3D image representations of tubular structures like in a dendritic tree. The derivative based methods allow accurate determination of centre line position and diameter even when they are blurred by the PSF of the imaging system.

The centre line detection method turned out to be applicable in confocal images of tubular structures in biological samples. The non-zero size of the kernels ensures derivative values that are based on a small volume in the neighbourhood of the position where the derivative has to be estimated. Consequently, the robustness of the centre line detection with respect to noise and irregularities is guaranteed by the utilization of these derivative kernels.

The method used for diameter measurement is essentially independent of scale of the derivative kernels as long as *a priori* knowledge on the shape of the intensity profile across the tube is present. The method has negligible bias as long as the sampling of the line structure is larger than approximately 2 voxels. The method fails when the size of the microscope PSF becomes of the order of magnitude of the diameter of the tubular structure. Bias starts to be significant when the lateral size of the PSF is as small as 20% of the diameter of the tube. We showed that it is possible to get an unbiased diameter estimate by incorporating the PSF in the diameter estimation method. The diameter value turns out to be unbiased even in the presence of considerable levels of background noise.

The results presented validate our approach in solving the problem of accurate centre line detection and diameter measurement in neuronal segments. By taking the microscope PSF into account more accurate detection of segment diameter is possible. Ignoring the microscope PSF which is common practice in existing systems will lead to erroneous diameter values.

Future research will have to be devoted to testing and tuning of the methods to ensure adequate measurement of basic morphological features of neurons from 3D confocal image data.

References

[1] Costa L Da F, Cesar R M, Coelho R C and Tanaka J S 1999 Analysis and synthesis of morphologically realistic neural networks *Modeling in the Neurosciences, from Ionic Channels to Neural Networks* ed R R Poznanski (Australia: Harwood Academic) pp 505–27

[2] Cesar R M and Costa L Da F 1997 Application and assessment of multiscale bending energy for morphometric characterization of neural cells *Rev. Sci. Instrum.* **68** 2177–86

[3] Costa L Da F and Velte T J 1999 Automatic characterization and classification of ganglion cells from the salamander retina *J. Comput. Neurol.* **404** 33–51

[4] Mascio L N, Verbeek P W, Sudar D, Kuo W L and Gray J W 1995 Semiautomated DNA-probe mapping using digital imaging microscopy. 1. System-development *Cytometry* **19** 51–9

[5] Ge Y R, Stelts D R, Wang J and Vining D J 1999 Computing the centerline of a colon: a robust and efficient method based on 3D skeletons *J. Comput. Assist. Tomogr.* **23** 786–94

[6] Brakenhoff G J, Blom P and Barends P 1979 Confocal scanning light microscopy with high aperture immersion lenses *J. Microsc.* **117** 219–32

[7] Koenderink J J and van Doorn A J 1994 Two-plus-one-dimensional differential geometry *Pattern Recognit. Lett.* **15** 439–43

[8] Steger C 1998 An unbiased detector of curvilinear structures *IEEE Trans. Pattern Anal. Mach. Intell.* **20** 113–25
[9] Steger C 1998 Unbiased extraction of curvilinear structures from 2D and 3D images *PhD Thesis* University of Munich
[10] Streekstra G J, Smeulders A W M and van den Boomgaard R 2000 Scale dependent differential geometry for the measurement of centerline and diameter in 3D curvilinear structures *Proc. 6th European Conf. on Computer Vision (Dublin)* (Berlin: Springer) pp 856–70
[11] Streekstra G J, Smeulders A W M and van den Boomgaard R 2001 Scale depencency of image derivatives for feature measurement in curvilinear structures *Int. J. Comput. Vis.* **42** 177–89
[12] Koller Th M, Gerig G, Szekely G and Dettwiler D 1995 Multiscale detection of curvilinear structures in 2D and 3D image data *Proc. 5th Int. Conf. on Computer Vision (Cambridge, MA)* (Los Alamitos, CA: IEEE Computer Society Press) pp 864–9
[13] Lorenz C, Carlsen I C, Buzug T M, Fassnacht C and Weese J 1997 Multi-scale line segmentation with automatic estimation of width, contrast and tangential direction in 2D and 3D medical images *Proc. 1st Joint Conf. on Computer Vision, Virtual Reality and Robotics in Medicine and Medical Robotics and Computer-Assited Surgery (Grenoble)* (Berlin: Springer) pp 233–42
[14] Lindeberg T 1994 *Scale-Space Theory in Computer Vision* (Boston, MA: Kluwer Academic)
[15] Kuijper A and Florack L M J 1999 Calculations on critical points under Gaussian blurring *Proc. 2nd Int. Conf. on Scale-Space Theories in Computer Vision (Corfu)* (Berlin: Springer) pp 318–29
[16] Sporring J, Nielsen M, Florack L and Johansen P 1997 *Gaussian Scale-Space Theory* (Boston, MA: Kluwer Academic)
[17] van Vliet L J 1993 Grey-scale measurements in multi-dimensional images *PhD Thesis* Delft University of Technology
[18] Bergsma C B J, Streekstra G J, Smeulders A W M and Manders E M M 2001 Velocity estimation of spots in three-dimensional confocal image sequences of living cells *Cytometry* **43** 261–72